Influence of Surface Area on Charge Transport and Recombination in Dye-Sensitized TiO_2 Solar Cells†

Kai Zhu, Nikos Kopidakis, Nathan R. Neale, Jao van de Lagemaat, and Arthur J. Frank*

National Renewable Energy Laboratory, 1617 Cole Boulevard, Golden, Colorado 80401-3393

Received: August 15, 2006; In Final Form: September 27, 2006

The dependence of the electron transport and recombination dynamics on the internal surface area of mesoporous nanocrystalline TiO_2 films in dye-sensitized solar cells was investigated. The internal surface area was varied by altering the average particle size in the films. The scaling of the photoelectron density and the electron diffusion coefficient at short circuit with internal surface area confirms the results of a recent study (Kopidakis, N.; Neale, N. R.; Zhu, K.; van de Lagemaat, J.; Frank, A. J. *Appl. Phys. Lett.* **2005**, *87*, 202106) that transport-limiting traps are located predominately on the surfaces of the particles. The recombination current density was found to increase superlinearly (with an exponent of 1.40 ± 0.12) with the internal surface area. This result is at odds with the expected linear dependence of the recombination current density on the surface area when only the film thickness is increased. The observed scaling of the recombination current density with surface area is consistent with recombination being transport-limited. Evidence is also presented confirming that photoinjected electrons recombine with redox species in the electrolyte via surface states rather than from the TiO_2 conduction band.

Introduction

Dye-sensitized solar cells (DSSCs; Grätzel cells) are considered one of the promising solar cell technologies of the future. Traditionally, DSSCs utilize a mesoporous nanocrystalline TiO_2 film covered with ruthenium-bipyridyl-based dyes as the photoelectrode material and triodide/iodide as the redox relay in the electrolyte. Such cells have reached conversion efficiencies above 11% at AM 1.5 solar irradiance.[1,2] An important feature of efficient DSSCs is their high light-harvesting efficiencies associated with monolayer dye coverage on large surface area films. Typically, the internal surface area of films is 2−3 orders of magnitude larger than their projected area. Often a film's surface area is increased to improve the light-harvesting efficiency. Under normal cell operating conditions, a major electron loss mechanism involves the recombination of photoinjected electrons with redox species in the electrolyte.[3,4] The rate of this process increases with increasing surface area, and thus, at some surface area value, the number of electrons recombining at the TiO_2/electrolyte interface becomes significant with respect to the number of electrons reaching the collecting electrode, resulting in a decreased solar conversion efficiency.[5−7] At open circuit, the recombination current density (and rate of recombination) can be determined from the short-circuit photocurrent density at the same illumination intensity.[8,9] For traditional DSSCs, it is generally assumed that the recombination current density scales linearly with surface area when the film thickness is varied and the average size of the nanocrystals is fixed. However, virtually nothing is known about the dependence of the recombination current density on the surface area for a fixed film thickness.

The recombination current density is expected to have a different dependence on the surface area, contingent upon whether recombination is limited by electron transport or the reaction of electrons with oxidized redox species at either the particle/electrolyte interface or the substrate/electrolyte interface. All of these processes are affected by the concentration of photoinjected electrons in the film, which, in turn, depends on the light intensity. The rate of recombination displays a power-law dependence on the photoelectron density. Several kinetic models have been proposed to account for this power-law dependence.[4,10−13]

It is widely accepted that electron transport in nanocrystalline TiO_2 films is limited by trapping and detrapping processes.[14−20] This phenomenon has been effectively described by a model in which electrons perform an exclusive random walk in a network of localized sites that have a power-law distribution of waiting (release) times.[18,21] This power-law distribution is generally attributed to energetic disorder arising from the presence of an exponential conduction band tail.[8,10,18,22] However, the physical explanation for the waiting-time distribution (WTD) is a subject of debate.[23−25] Regardless of the physical origin of the distribution, we recently showed that transport-limiting traps are located predominately on the particle surface.[26]

In this paper, we present results of our investigation on the effect of surface area on recombination when the average particle size in TiO_2 films is varied while keeping the film thickness and porosity constant. Analyses of intensity-modulated photovoltage spectroscopy (IMVS) measurements suggest that the recombination current density increases superlinearly with the surface area. This result contrasts with the expected linear dependence of recombination current density on the surface area when only the film thickness is increased. Three kinetic recombination models are considered to understand the origin of the nonlinear dependence of the recombination current density on photoelectron density. Intensity-modulated photocurrent spectroscopy (IMPS) and IMVS data are consistent with the transport-limited recombination model and with transport-limiting traps being located on the surfaces of the nanoparticles.

† Part of the special issue "Arthur J. Nozik Festschrift".

* Author to whom correspondence should be addressed. E-mail: afrank@nrel.gov.

10.1021/jp065284+ CCC: $33.50
Published on Web 11/09/2006

The results are also consistent with electrons recombining from surface states rather than from the TiO_2 conduction band.

Experimental Section

Sample Preparation. Dye-sensitized TiO_2 solar cells were fabricated as detailed elsewhere.[27,28] Mesoporous TiO_2 films were deposited via the doctor-blade technique using a paste of TiO_2 nanoparticles on a transparent conducting glass (TCO) substrate (LOF TEC8 F-doped SnO_2 glass; Hartford Glass Company). After the films were sintered at 450 °C in air for 30 min and cooled to 80 °C, they were immersed in an ethanolic solution containing 0.3 mM $TBA_2[RuL_2(NCS)_2]$ (L = 4-carboxylic acid-4′-carboxylate-2,2′-bipyridyl; TBA = tetrabutylammonium; commonly called N719 dye) for 24 h. The semitransparent counter electrode consisted of TCO covered with a Pt catalyst. The cells were filled with an electrolyte composed of 0.8 M 1-hexyl-2,3-dimethylimidazolium iodide and 50 mM iodine in methoxypropionitrile.

By varying the temperature of the autoclaving step in the nanoparticle synthesis, we obtained average particle sizes (r) between 20.5 and 41.5 nm, as determined by X-ray diffraction (XRD). Within the detection limit of the XRD experiment (<5%), only the TiO_2 anatase phase was observed. The roughness factor (rf) of the films ranged from 57 to 149 μm^{-1}, as determined by gas sorption measurements. The best fit to the particle size versus roughness factor data yields a dependence of $r \propto (\mathrm{rf})^{-0.8}$ for reasons discussed elsewhere.[26] The porosity (P) was 57.5% ± 1.5% for all films as determined with a Quantachrome NOVA 2000 high-speed nitrogen sorption surface and pore-size analyzer. The average TiO_2 film thickness was 11.7 ± 0.3 μm as measured with a surface profiler (KLA Tencor Alpha-Step 500).

Transport and Recombination Measurements. IMPS at short circuit was used to measure photocarrier transport times, as detailed elsewhere.[14−17,19,20,29−31] Photocarrier recombination times were measured at open circuit by IMVS.[8,10,30] A semiconductor diode laser (680 nm) was used to illuminate the sample from the substrate side; it served as both the bias illumination and the small sinusoidally modulated probe beam. IMPS and IMVS measurements were performed at modulation frequencies between 1 mHz and 10 kHz by a SR830 lock-in amplifier. Neutral density filters were used to vary the illumination intensity. The amplitude of the modulated photocurrent density was kept at 10% or lower compared to the steady-state photocurrent density. Details of the IMPS and IMVS measurements and data analysis are given in Appendix A.

Theory

Transport. The nonlinear dependence of the electron diffusion coefficient (D) on photoelectron density at short circuit (n_{sc}) has been modeled using an exclusive random walk on a grid of sites (traps) having a power-law distribution of waiting (release) times (WTD) in the form of $t^{-1-\alpha}$, where the parameter α is in the range between 0 and 1.[18,21] From the WTD, we have developed an analytic expression (eq B.4) that relates D to the total trap density (N_T) and to n_{sc}. This expression is used to calculate the absolute value of D as a function of N_T. Details of the derivation are given in Appendix B. Figure 1a shows the results of calculations with eq B.4 for $\alpha = 0.37$ for various values of n_{sc} and N_T. The electron diffusion coefficient is seen to exhibit the usual power-law dependence on the photoelectron density.[14−16,21,22,32,33] Also, it is seen that D decreases with increasing values of N_T in concurrence with experimental results.[26] Best fits of the data yield the power-law relation $D \propto (n_{sc})^{1.77}$. Figure 1b displays the dependence of D on N_T for a photoelectron density of 10^{16} cm^{-3} using data in Figure 1a. A power-law fit to the data yields the expression: $D \propto (N_T)^{-2.36}$. The same power-law dependence of D on N_T is observed for each value of n_{sc} displayed in Figure 1a.

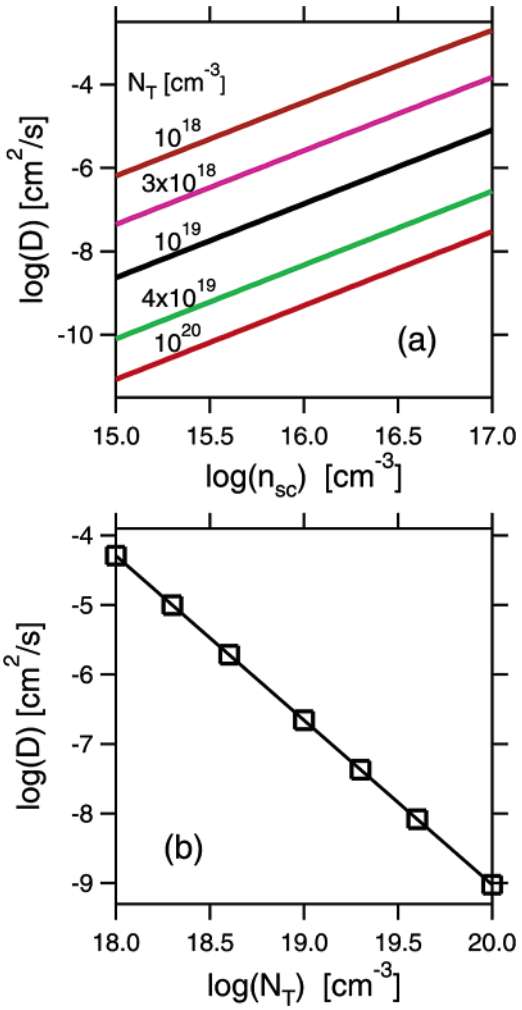

Figure 1. (a) Analytic calculations (eq B.4) of the dependence of the electron diffusion coefficient (D) on the photoelectron density (n_{sc}) at short circuit for various values of the total trap density (N_T). (b) Dependence of D on N_T at a photoelectron density of 10^{16} cm^{-3} using data from Figure 1a. The line is a best power-law fit to the data (squares).

Within the framework of the exclusive random walk model, an approximate relation between D and the total trap density has been derived[21]

$$D = C_1(N_T)^{-(1/\alpha)+(1/3)}(n_{sc})^{(1/\alpha)-1} \quad (1)$$

where C_1 is a constant that is independent of particle size. To derive eq 1, it is assumed that the average detrapping time of electrons can be approximated by the localization time for traps at the electron quasi-Fermi level. In contrast, to derive eq B.4 the localization times that are associated with all states are used to determine the average detrapping time of electrons (eq B.3). For $\alpha = 0.37$, eq 1 is in excellent agreement with the data in Figures 1a and 1b.

Using theory developed earlier,[21] one can derive the following expression for the photoelectron density n_{sc} at short circuit

$$n_{sc} = C_2 N_T (J_{sc})^{\alpha} \quad (2)$$

TABLE 1: Predicted Value of the Exponent (γ) for the Dependence of N_T, D, and n_{sc} on (rf)$^{\gamma}$ at Short Circuit

trap location	N_T	D	n_{sc}
surface	1	(1/3)−(1/α)	1
grain boundary	2.4	(0.8)−(2.4/α)	2.4
bulk	0	0	0

where C_2 is a constant, independent of particle size, and J_{sc} is the photocurrent density at short circuit.[26]

Recently, we showed that the scaling of N_T with the roughness factor rf depends on the spatial location of transport-limiting traps.[26] The roughness factor corresponds to the total surface area per volume of film (including voids). From the relationship between N_T and rf, the respective scaling dependences of D and n_{sc} on rf can be derived with the aid of eqs 1 and 2. Table 1 summarizes the dependence of N_T, D (at constant n_{sc}), and n_{sc} (at constant J_{sc}) on rf for traps located on the surfaces of particles, in their bulk, or at grain boundaries.

Recombination. The recombination current density J_r at open circuit can be equated to the short-circuit photocurrent density at the same light intensity.[8,9] (Note that at short circuit recombination is negligible.[21,22]) The recombination rate R at open circuit can be calculated from J_r using the expression $R = J_r/qd$, where q is the elementary charge and d is the film thickness. The apparent order of J_r (or R) on the photoelectron density n_{oc} at open circuit is controversial. It is usually reported to be approximately second-order[4,11,17,34] or higher.[4,17,34] Several kinetic models have been proposed to account for this nonlinear dependence of J_r on n_{oc}. One model, which we denote as model 1, attributes the second-order nature of J_r to a two-electron process[10,11]

$$J_r = k_1 n_{oc}^2 c_x \quad (3)$$

where k_1 is the rate constant and c_x is the volume density of surface recombination sites. In this model, k_1 is usually assumed to be independent of the energy levels of recombination sites.

The order of J_r on n_{oc} can also be explained by invoking a first-order rate constant k_2, which depends on the free energy difference between electrons in TiO_2 particles and the redox potential in the electrolyte; hereafter, we refer to this possibility as model 2. In this model, k_2 can be related to qV_{oc} (where V_{oc} is the open-circuit voltage) via Marcus−Gerischer or Butler−Volmer models.[12,35,36] In this case, the recombination current density can be expressed by

$$J_r = k_2 n_{oc} c_x \quad (4)$$

Inasmuch as changes in the photoelectron density in the film alter V_{oc}, k_2 implicitly depends on n_{oc}.

Recently, we showed that electron diffusion to surface sites controls recombination.[4] In this model (denoted as model 3), the dependence of J_r on n_{oc} is explained by assuming that the rate constant k_3 depends on the electron diffusion coefficient ($k_3 = k'D$, where k' is a constant). For this case, the recombination current density can be written as

$$J_r = k_3 n_{oc} c_x = k' D n_{oc} c_x = k' C_1 (n_{oc})^{1/\alpha} (N_T)^{(1/3)-(1/\alpha)} c_x \quad (5)$$

Because the electron diffusion coefficient depends on the photoelectron density (eq 1), k_3 also implicitly depends on n_{oc}.

Model 1 differs from models 2 and 3 since it assumes that the recombination reaction is always second-order in photoelectron density. Because, as discussed above, both k_2 and k_3 implicitly depend on n_{oc}, the experimentally measurable quantities V_{oc} (model 2) and D (model 3) are connected. Therefore, it is not possible to distinguish between models 2 and 3 by studying the dependence of J_r on V_{oc} and D. A parameter that does differentiate between models 2 and 3 is the roughness factor rf. Changes in rf are expected to result in different scaling of J_r, depending on the kinetic model.

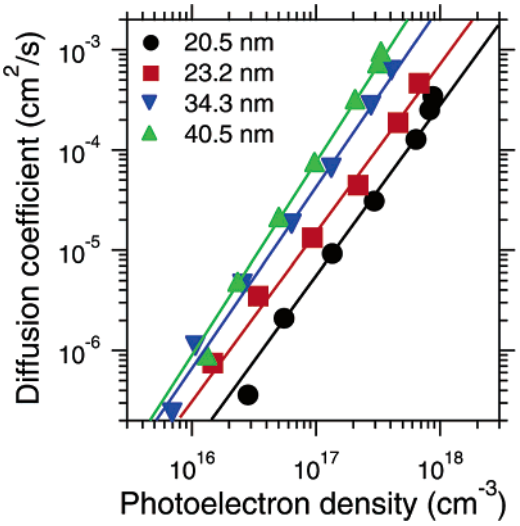

Figure 2. Dependence of the electron diffusion coefficient on the photoelectron density at short circuit for DSSCs composed of films having different average-sized particles. Lines are best fits to eq 1. The electron density was calculated using eq A.3.

Assuming a uniform areal density of recombination sites, it follows that the volume density of recombination sites c_x is proportional to the roughness factor per unit of film thickness (since the film thickness is held constant, $c_x \propto$ rf). As discussed above, N_T scales differently with rf, depending on the spatial location of transport-limiting traps (Table 1). Similarly, n_{oc} scales differently with rf, depending on the spatial location of photoinduced electrons at open circuit. Therefore, a study of the dependence of J_r versus rf can reveal which of the three kinetic recombination models predominates in DSSCs.

A related mechanistic issue is the electronic states from which photogenerated electrons recombine with oxidized redox species. In principle, electrons can recombine with the redox electrolyte either from the conduction band or from surface states. Although this topic was first addressed sometime ago,[8] it is still a matter of debate.[8,10,30,32,35,37−39] By studying the scaling dependence of J_r on V_{oc} ($J_r \propto \exp(qV_{oc}/m_0)$),[8] one can distinguish between these two mechanisms.[8,30,37] The value of the parameter m_0, the inverse of the slope of the plot of J_r versus $\ln(qV_{oc})$, is a measure of the scaling dependence. If electrons recombine primarily from the conduction band, then all three models predict $m_0 \leq k_B T$, where k_B is the Boltzmann constant and T is the temperature.[8,30] The $k_B T$ term reflects the relationship between the free electron density and the quasi-Fermi level (qV_{oc}), which is determined by the light intensity. However, if electrons recombine mainly via surface states, then m_0 is greater than $k_B T$.[8,30] In this case, m_0 can be related to the WTD parameter α for electron transport.

Results and Discussion

Transport. Figure 2 shows that the electron diffusion coefficient D displays a power-law dependence on the photoinduced electron density n_{sc} at short circuit (eq 1). Such a power-law relationship has been observed previously.[14−16,21,22] The best fits of the data to eq 1 yield the WTD parameter $\alpha = 0.35 \pm 0.02$ for all samples. The data indicate that electrons move faster

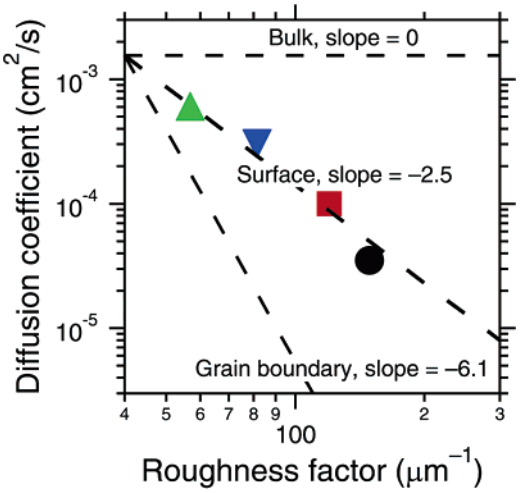

Figure 3. Dependence of the electron diffusion coefficient on the roughness factor at a photoelectron density of 3×10^{17} cm^{-3}. The symbols correspond to films with different particle sizes as indicated in Figure 2. The lines represent predictions from the three kinetic models (Table 1).

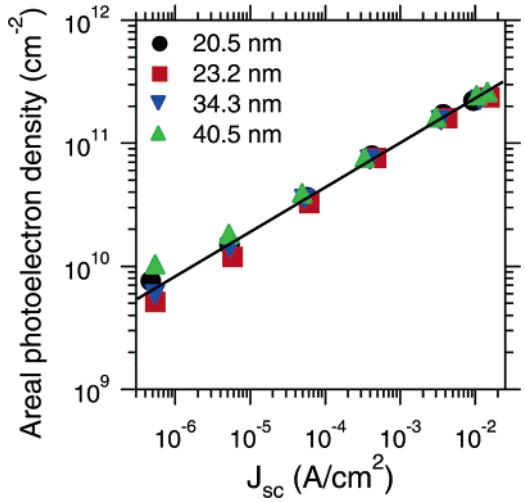

Figure 4. Dependence of the areal photoelectron density on the short-circuit photocurrent density. The areal photoelectron densities are normalized with respect to the roughness factor of sensitized films composed of different average-sized particles. The line is the best fit.

as the particle size increases or, equivalently, as the roughness factor decreases, in agreement with a recent study.[26]

From Table 1 and the plots in Figure 2, one can determine the relationship between D and rf at a given n_{sc} value and, therefore, identify the spatial location of the traps. Figure 3 displays a plot of the electron diffusion coefficient versus roughness factor at some constant value of photoelectron density ($n_{sc} = 3 \times 10^{17}$ cm^{-3}); D was determined from the best-fit lines in Figure 2. The predictions of the three models (Table 1) are also compared for $\alpha = 0.35$. The best fit of the data indicates that $D \propto (\mathrm{rf})^{-2.9\pm0.3}$. From a comparison of the predictions of the three models (Figure 3 or Table 1), it can be concluded that transport-limiting traps are located mainly on the surfaces of the TiO_2 particles. This result agrees with a previous study that covered 1 order of magnitude change in light intensity.[26] For other fixed values of photoelectron densities, which range from 10^{16} to 3×10^{17} cm^{-3}, corresponding to more than 4 orders of magnitude of light intensity, the same conclusion is reached.

Figure 4 shows a plot of the areal photoelectron density n_{sc}^{s} versus the short-circuit photocurrent density J_{sc} (representing the incident light intensity) for DSSCs composed of films with

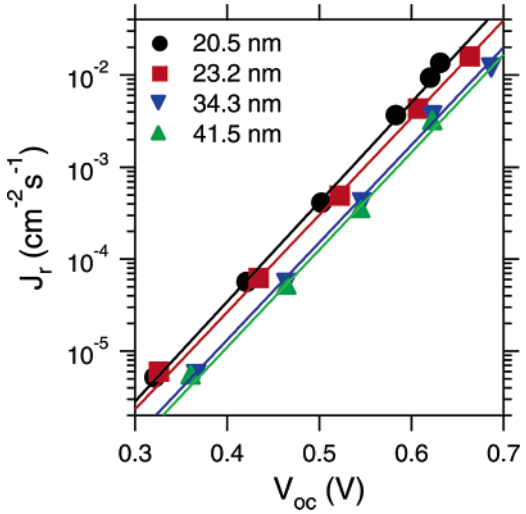

Figure 5. Dependence of the recombination current density on the open-circuit photovoltage for DSSCs composed of films having different average-sized particles. Lines are the best fits with exponential dependences.

different average particle sizes; the areal photoelectron density was calculated from the relation $n_{sc}^{s} = n_{sc}(1 - P)/\mathrm{rf}$, where P is the film porosity, which is 57.5%. The plots of n_{sc}^{s} versus J_{sc} coincide, which indicates that the photoelectron densities for the films with four different average particle sizes scale linearly with their surface area for over 4 orders of magnitude change in J_{sc}; the values for J_{sc} correspond to those measured for DSSCs for light intensities ranging from about 10^{-4} suns to 1 sun. The parameter α obtained from the best fit (line in Figure 4) is 0.35, which is the same value of α obtained from fits of D versus n_{sc} in Figure 2. From Table 1, the direct proportionality between n_{sc} and rf reaffirms that the photoinjected electrons reside mainly on the surface of the particles during transport, instead of in the particle bulk or at grain boundaries, in agreement with our previous results.[26] This result also shows that n_{sc} is directly proportional to the total trap density N_T at constant J_{sc} (eq 2).

Recombination. Figure 5 displays the recombination current density J_r as a function of the open-circuit voltage V_{oc} for films composed of different average-sized particles. The recombination current density increases over 4 orders of magnitude when V_{oc} ranges from 0.3 to 0.7 V. It can be seen that recombination becomes faster with decreasing particle size or, equivalently, with increasing roughness factor for each value of V_{oc}. The recombination current density for all samples follows the same exponential dependence on V_{oc} over the voltage range displayed. The best fit of the slopes of the plots (m_0) in Figure 5 is about 40 meV, which is within the range reported previously.[10,12,16,30,39,40] Because the measured value of m_0 is significantly larger than k_BT (Theory section), we conclude that, for the light intensity range displayed in Figure 5, electrons recombine via surface states instead of from conduction band states in concurrence with the conclusion of other studies.[8,30]

For $V_{oc} < 0.3$ V (not shown), corresponding to illumination levels less than 10^{-4} suns, J_r does not follow the same dependence on V_{oc} as observed for the plots in Figure 5. Differences in J_r among the samples become less significant, suggesting that recombination occurs primarily at the surface of the TCO substrate.[31,38]

Figure 6 shows the dependence of the areal photoelectron density n_{oc}^{s} on V_{oc}. The n_{oc}^{s} values are essentially the same between 0.3 and 0.6 V for the films with different roughness

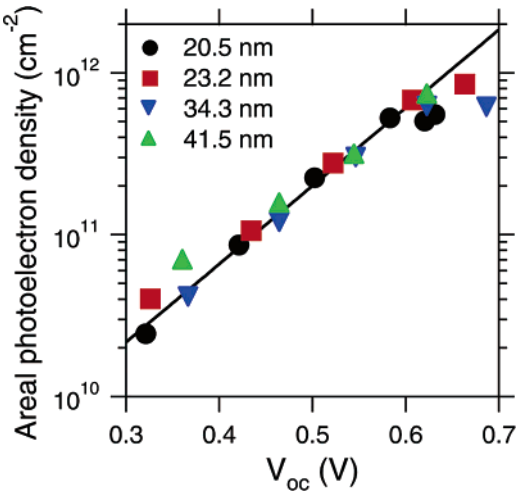

Figure 6. Dependence of the areal photoelectron density on the open-circuit photovoltage for DSSCs composed of films having different average-sized particles. The line is the best fit with an exponential dependence between 0.3 and 0.6 V.

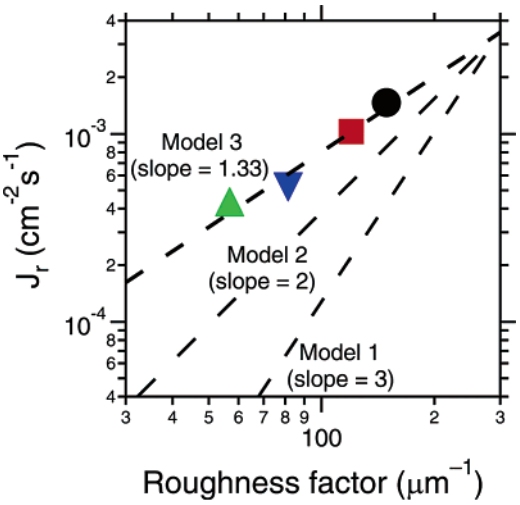

Figure 7. Dependence of the recombination current density on the roughness factors at $V_{oc} = 0.55$ V for DSSCs composed of films having different average-sized particles. Symbols correspond to films with different particle sizes as indicated in Figure 2. Dashed lines represent predictions based on three kinetic models (Theory section).

factors, indicating that the photoelectron density is directly proportional to the film roughness factor and, therefore, that the photoinjected electrons are located mainly on the surface of the particles at open circuit. The line represents exponential fits. The small deviation of the plot from the fitted exponential dependence at $V_{oc} > 0.6$ V is attributed to the band-edge shift arising from charging of the Helmholtz layer at the TiO_2 particle/electrolyte interface.[41,42] As a result, V_{oc} increases more rapidly with increasing photoelectron density than would be expected for an exponential dependence of n_{oc}^{s} on V_{oc}. Despite this deviation, the normalized photoelectron density values remain close among samples with differing roughness factors.

Figure 7 displays a plot of the recombination current density versus roughness factor at some constant value of V_{oc} ($V_{oc} = 0.55$ V). The values of J_r were determined from the best fit in Figure 5. The three dashed lines in Figure 7 represent predictions based on the three kinetic models to explain the order of J_r on n_{oc} (Theory section). From the dependences of c_x, N_T, and n_{oc} on rf, the recombination current density is predicted to be proportional to $(rf)^3$ for model 1 (eq 3), to $(rf)^2$ for model 2 (eq 4), and to $(rf)^{1.33}$ for model 3 (eq 5). Model 1 assumes that the rate constant for recombination k_1 is invariant and that interfacial charge-transfer processes involve two electrons. In model 2, it is assumed that J_r is first-order in the photoelectron density and that the rate constant k_2 depends on V_{oc}. However, because V_{oc} is fixed, k_2 becomes a constant. Model 3 assumes that J_r is first-order in the photoelectron density and that the rate constant k_3 scales with the electron diffusion coefficient D.[4] Because D depends on the photoelectron density (eq 1), k_3 *also depends* on n_{oc}. From the best fit of the experimental data to $J_r \propto (rf)^{\gamma}$, we find that the exponent value $\gamma = 1.40 \pm 0.12$, which is consistent with model 3, implying that recombination is transport-limited. The same conclusion is reached for other fixed values of V_{oc} (Figure 5).

Conclusion

We investigated the influence of the internal surface areas of sensitized mesoporous nanocrystalline TiO_2 films on electron transport and recombination by IMPS and IMVS. The surface area was changed by varying the average particle size in the films while keeping the film thickness and porosity constant. The scaling of the photoelectron density and the electron diffusion coefficient at short circuit with internal surface area confirms the results of a recent study[26] that transport-limiting traps are located mainly on the surfaces of the particles. We find that the recombination current density increases superlinearly with the surface area. This result contrasts with the expected linear increase of the recombination current density with the surface area when the film thickness is increased. The nonlinear dependence of the recombination current density on electron density was found to be consistent with transport-limited recombination. The measurements also confirmed that electrons recombine via surface states rather than from the TiO_2 conduction band.[8]

Acknowledgment. This work was supported by the Office of Science, Division of Chemical Sciences, and the Office of Utility Technologies, Division of Photovoltaics, U. S. Department of Energy, under Contract No. DE-AC36-99GO10337.

Appendix A: Transport and Recombination Measurements

At low modulation frequencies, the IMPS response function T can be approximated by[41]

$$T = A\frac{1}{1 + i\omega\tau_c} \tag{A.1}$$

where ω is the angular frequency of modulation, τ_c is the characteristic time constant, and A is the magnitude of the IMPS response at $\omega = 0$. The effective electron diffusion coefficient D can be calculated from[21,41]

$$D = \frac{d^2}{(2.35\tau_c)} \tag{A.2}$$

where d is the film thickness. The photocarrier density at short circuit n_{sc} established by the bias light illumination is determined from[42]

$$n_{sc} = \frac{T_n J_{sc} \tau_c}{qd(1 - P)} \tag{A.3}$$

where T_n is a thermodynamic factor,[42] q is the elementary charge, J_{sc} is the short-circuit photocurrent density, and P is the film porosity.

The IMVS response is normally a semicircle when plotted in the complex plane. The electron lifetime constant τ_r can be calculated from $\tau_r = 1/\omega_{min}$,[8,10] where ω_{min} is the characteristic angular frequency where the imaginary component of IMVS reaches its minimum value. The photocarrier density n_{oc} at open circuit was calculated from[4]

$$n_{oc} = \frac{J_{sc}\tau_r}{qd(1-P)} \tag{A.4}$$

Appendix B: Theoretical Treatment of Electron Transport in TiO_2 Nanoparticle Films

Analytical expressions are calculated for the electron diffusion coefficient using a continuous-time random walk approach. The (tracer)[42] electron diffusion coefficient D is related to the mean localization time $\bar{t}$ and the root-mean-square distance between localized sites (traps) λ via the Einstein−Schmoluchowski relation[43]

$$D = \frac{\lambda^2}{6\bar{t}} \tag{B.1}$$

The parameter λ is defined by the relation

$$\lambda^2 = \sum_{\vec{s}} s^2 p(\vec{s})$$

where $\vec{s}$ is a vector that connects localization sites, s is its length, and $p(\vec{s})$ is the normalized probability for an electron to follow $\vec{s}$. In the case of mesoporous nanocrystalline TiO_2 films, λ is approximately equal to the average distance between *neighboring* localization sites (traps) and is expressed by the relation $\lambda \approx N_T^{-1/3}$, where N_T is the total density of traps.[21] It is noteworthy that N_T represents the total density of traps per film volume, while another related parameter, the average number of traps per particle, can be estimated from $N_T V_r/(1-P)$, where V_r is the average volume of TiO_2 particles and the interconnected volume between particles is ignored. Assuming that the time it takes for an electron to travel from trap-to-trap is negligible with respect to the localization time, that the WTD is described by the (normalized) power-law form $\psi(t) = \alpha\nu^{-\alpha}\theta(t-\nu^{-1})t^{-1-\alpha}$, that the random walk over the localization sites is exclusive (no more than one electron can occupy a certain site at any moment in time), and that the density of carriers is small with respect to the number of sites, it can be shown by simple statistical arguments that at steady state, where there is a constant electron density in the film, the distribution of localization times $\psi(t)$ has the form

$$\psi(t) = \frac{(\alpha+1)\nu^{-1-\alpha}}{{}_2F_1(1,\alpha+1;\alpha+2;-t_F\nu)}\frac{\theta(t-\nu^{-1})t^{-1-\alpha}}{(t_F+t)} \tag{B.2}$$

where α ranges between 0 and 1 and ν is the highest possible release frequency from a localization site. Equation B.2 is characterized by two power laws and an inflection point at a characteristic time t_F (denoted hereafter as the Fermi time) that in a trapping model with energetic disorder corresponds to the emission time of a trap at the Fermi energy. The parameter α is a measure of disorder in the material.[23] The parameter ν in a trapping model would correspond to the thermal frequency, which typically ranges from 10^{12} to 10^{13} s^{-1} and is related, via detailed balance, to the capture cross-section of the traps. The second fraction on the right in eq B.2 describes the distribution of localization times, and the first fraction on the right ensures that the distribution is normalized to unity. The term $\theta(t)$ is the elementary step function, and ${}_2F_1$ is a hypergeometric function defined by the series expansion ${}_2F_1(a,b;c;z) = \sum_{k=0}^{\infty}(a)_k(b)_k(c)_k^{-1}z^k(k!)^{-1}$. When mapped to a trapping model with energetic disorder, eq B.2 requires that the capture cross-section of traps does not depend on the trap depth (i.e., the thermal frequency is not a function of trap depth). The power-law expression in the numerator of eq B.2 is the same as that first introduced by Scher and Montroll[44] to explain transport in amorphous semiconductors. In a multiple-trapping-type explanation for eq B.2, the $(t_F + t)$ term in the denominator accounts for the diminished occurrence of long emission times as the result of the presence of a quasi-Fermi level for electrons established by the bias light.

The mean localization time $\bar{t}$ is determined by averaging all localization times over the distribution $\psi(t)$

$$\bar{t} = \int_0^{\infty} t\psi(t)\,dt = -\frac{t_F B_{-t_F\nu}(\alpha,0)}{B_{-t_F\nu}(\alpha+1,0)} \tag{B.3}$$

where $B_z(c,d)$ is the incomplete beta function defined by the equation

$$B_z(c,d) = \int_0^z x^{c-1}(1-x)^{d-1}\,dx$$

The steady-state (tracer) diffusion coefficient of electrons, corresponding to complete thermalization, is calculated with the aid of eqs B.1 and B.3

$$D = \frac{\lambda^2}{6\bar{t}} = -\frac{\lambda^2 B_{-t_F\nu}(\alpha+1,0)}{6t_F B_{-t_F\nu}(\alpha,0)} \tag{B.4}$$

Equation B.4 provides an analytical expression for the tracer diffusion coefficient of electrons in TiO_2 under constant bias light. It can be used to calculate the dependence of the effective (chemical) diffusion coefficient of electrons on photoinduced charge density and total trap density by simply multiplying eq B.4 by the thermodynamic factor, which equals $1/\alpha$.[42]

In an earlier paper,[21] we derived an approximate relation for D that is within 5% of eq B.4 for typical values of t_F and α. Equation B.4 shows that the steady-state diffusion coefficient of electrons is determined by the Fermi time and the slope of the WTD. To a first approximation, D is inversely proportional to t_F. The same dependence of D on t_F can be inferred from an electron-transport modeling study[45] that assumes that only states at the Fermi level are important.

References and Notes

(1) Grätzel, M. *J. Photochem. Photobiol., A* **2004**, *164*, 3.
(2) Chiba, Y.; Islam, A.; Watanabe, Y.; Komiya, R.; Koide, N.; Han, L. Y. *Jpn. J. Appl. Phys.* **2006**, *45*, L638.
(3) Gregg, B. A.; Pichot, F.; Ferrere, S.; Fields, C. L. *J. Phys. Chem. B* **2001**, *105*, 1422.
(4) Kopidakis, N.; Benkstein, K. D.; van de Lagemaat, J.; Frank, A. J. *J. Phys. Chem. B* **2003**, *107*, 11307.
(5) Hara, K.; Horiguchi, T.; Kinoshita, T.; Sayama, K.; Sugihara, H.; Arakawa, H. *Sol. Energy Mater. Sol. Cells* **2000**, *64*, 115.
(6) Kang, M. G.; Ryu, K. S.; Chang, S. H.; Park, N. G.; Hong, J. S.; Kim, K. J. *Bull. Korean Chem. Soc.* **2004**, *25*, 742.
(7) Ito, S.; Kitamura, T.; Wada, Y.; Yanagida, S. *Sol. Energy Mater. Sol. Cells* **2003**, *76*, 3.
(8) Schlichthörl, G.; Huang, S. Y.; Sprague, J.; Frank, A. J. *J. Phys. Chem. B* **1997**, *101*, 8141.

(9) Kopidakis, N.; Neale, N. R.; Frank, A. J. *J. Phys. Chem. B* **2006**, *110*, 12485.
(10) Fisher, A. C.; Peter, L. M.; Ponomarev, E. A.; Walker, A. B.; Wijayantha, K. G. U. *J. Phys. Chem. B* **2000**, *104*, 949.
(11) Duffy, N. W.; Peter, L. M.; Rajapakse, R. M. G.; Wijayantha, K. G. U. *J. Phys. Chem. B* **2000**, *104*, 8916.
(12) Huang, S. Y.; Schlichthörl, G.; Nozik, A. J.; Grätzel, M.; Frank, A. J. *J. Phys. Chem. B* **1997**, *101*, 2576.
(13) Nelson, J.; Haque, S. A.; Klug, D. R.; Durrant, J. R. *Phys. Rev. B* **2001**, *63*, 205321.
(14) Cao, F.; Oskam, G.; Meyer, G. J.; Searson, P. C. *J. Phys. Chem.* **1996**, *100*, 17021.
(15) de Jongh, P. E.; Vanmaekelbergh, D. *Phys. Rev. Lett.* **1996**, *77*, 3427.
(16) Dloczik, L.; Ileperuma, O.; Lauermann, I.; Peter, L. M.; Ponomarev, E. A.; Redmond, G.; Shaw, N. J.; Uhlendorf, I. *J. Phys. Chem. B* **1997**, *101*, 10281.
(17) Schlichthörl, G.; Park, N. G.; Frank, A. J. *J. Phys. Chem. B* **1999**, *103*, 782.
(18) Nelson, J. *Phys. Rev. B* **1999**, *59*, 15374.
(19) van de Lagemaat, J.; Frank, A. J. *J. Phys. Chem. B* **2000**, *104*, 4292.
(20) Kambili, A.; Walker, A. B.; Qiu, F. L.; Fisher, A. C.; Savin, A. D.; Peter, L. M. *Physica E* **2002**, *14*, 203.
(21) van de Lagemaat, J.; Frank, A. J. *J. Phys. Chem. B* **2001**, *105*, 11194.
(22) Kopidakis, N.; Schiff, E. A.; Park, N. G.; van de Lagemaat, J.; Frank, A. J. *J. Phys. Chem. B* **2000**, *104*, 3930.
(23) Kopidakis, N.; Benkstein, K. D.; van de Lagemaat, J.; Frank, A. J.; Yuan, Q.; Schiff, E. A. *Phys. Rev. B* **2006**, *73*, 045326.
(24) O'Regan, B. C.; Durrant, J. R. *J. Phys. Chem. B* **2006**, *110*, 8544.
(25) Peter, L. M.; Walker, A. B.; Boschloo, G.; Hagfeldt, A. *J. Phys. Chem. B* **2006**, *110*, 13694.
(26) Kopidakis, N.; Neale, N. R.; Zhu, K.; van de Lagemaat, J.; Frank, A. J. *Appl. Phys. Lett.* **2005**, *87*, 202106.
(27) Benkstein, K. D.; Kopidakis, N.; van de Lagemaat, J.; Frank, A. J. *J. Phys. Chem. B* **2003**, *107*, 7759.
(28) Neale, N. R.; Kopidakis, N.; van de Lagemaat, J.; Grätzel, M.; Frank, A. J. *J. Phys. Chem. B* **2005**, *109*, 23183.
(29) de Jongh, P. E.; Vanmaekelbergh, D. *J. Phys. Chem. B* **1997**, *101*, 2716.
(30) van de Lagemaat, J.; Park, N. G.; Frank, A. J. *J. Phys. Chem. B* **2000**, *104*, 2044.
(31) Zhu, K.; Schiff, E. A.; Park, N. G.; van de Lagemaat, J.; Frank, A. J. *Appl. Phys. Lett.* **2002**, *80*, 685.
(32) Nakade, S.; Saito, Y.; Kubo, W.; Kitamura, T.; Wada, Y.; Yanagida, S. *J. Phys. Chem. B* **2003**, *107*, 8607.
(33) Boschloo, G.; Haggman, L.; Hagfeldt, A. *J. Phys. Chem. B* **2006**, *110*, 13144.
(34) Schlichthörl, G.; Park, N. G.; Frank, A. J. *Z. Phys. Chem.* **1999**, *212*, 45.
(35) Salvador, P.; Hidalgo, M. G.; Zaban, A.; Bisquert, J. *J. Phys. Chem. B* **2005**, *109*, 15915.
(36) Bisquert, J.; Zaban, A.; Greenshtein, M.; Mora-Sero, I. *J. Am. Chem. Soc.* **2004**, *126*, 13550.
(37) Bisquert, J.; Zaban, A.; Salvador, P. *J. Phys. Chem. B* **2002**, *106*, 8774.
(38) Cameron, P. J.; Peter, L. M.; Hore, S. *J. Phys. Chem. B* **2005**, *109*, 930.
(39) Park, N. G.; Schlichthörl, G.; van de Lagemaat, J.; Cheong, H. M.; Mascarenhas, A.; Frank, A. J. *J. Phys. Chem. B* **1999**, *103*, 3308.
(40) Södergren, S.; Hagfeldt, A.; Olsson, J.; Lindquist, S. E. *J. Phys. Chem.* **1994**, *98*, 5552.
(41) Frank, A. J.; Kopidakis, N.; van de Lagemaat, J. *Coord. Chem. Rev.* **2004**, *248*, 1165.
(42) van de Lagemaat, J.; Kopidakis, N.; Neale, N. R.; Frank, A. J. *Phys. Rev. B* **2005**, *71*, 035304.
(43) Scher, H.; Lax, M. *Phys. Rev. B* **1973**, *7*, 4491.
(44) Scher, H.; Montroll, E. W. *Phys. Rev. B* **1975**, *12*, 2455.
(45) Vanmaekelbergh, D.; de Jongh, P. E. *Phys. Rev. B* **2000**, *61*, 4699.